Matrix formalism for radiating polarization sheets in multilayer structures of arbitrary composition

Hui Shi (石 卉), Yu Zhang (张 雨), Hongqing Wang (王洪庆), and Weitao Liu (刘韡韬)*

Physics Department, State Key Laboratory of Surface Physics, Key Laboratory of Micro and Nano Photonic Structures (MOE), Collaborative Innovation Center of Advanced Microstructures (Nanjing), Fudan University, Shanghai 200433, China

corresponding author: wtliu@fudan.edu.cn

In optical studies on layered structures, quantitative analysis of radiating interfaces is often challenging due to multiple interferences. We present here a general and analytical method for computing the radiation from two-dimensional polarization sheets in multilayer structures of arbitrary compositions. It is based on the standard characteristic matrix formalism of thin films, and incorporates boundary conditions of interfacial polarization sheets. We use the method to evaluate the second harmonic generation from a nonlinear thin film, and the sum-frequency generation from a water/oxide interface, showing that the signal of interest can be strongly enhanced with optimal structural parameters.

OCIS codes: 190.4400, 260.3160, 310.4165, 310.6860.

doi: 10.3788/COL201715.081901.

Multilayer structures of thin films are indispensable in modern technology and scientific research[1–5]. In such structures, interfaces often play a key role: they give rise to desirable electronic and optoelectronic functions[6], and are the host of many novel phenomena[7]. Across the interfaces, the broken symmetry often causes a net polar ordering, which is readily monitored by surface-specific optical techniques. For example, second-order nonlinear optical processes such as second harmonic generation (SHG) and sum-frequency generation (SFG) can be highly surface sensitive for centrosymmetric media, and are widely employed in interfacial studies[8–12]. Experimentally, the optical signal depends on both the interfacial polarizations and local electric fields[13,14]. Yet, due to the coexistence of multiple interfaces and the interference between multiply reflected beams[15], it is often challenging to perform quantitative analysis[16,17].

In this study, we introduce a method for computing the radiation from interfacial polarization sheets in multilayer structures. Our method is based on the standard characteristic matrix formalism of thin films[16,17], and incorporates boundary conditions of electromagnetic fields due to such polarization sheets[18]. It yields the contribution of each individual interface, and applies to multilayer structures of arbitrary composition. With this analytical approach, we can easily choose appropriate structural parameters to selectively boost up or suppress responses from specific locations. We present here two practical examples showing that appropriate geometries can strongly enhance the response from thin films or interfaces of interest. This method is not limited to nonlinear optical studies, but is generally applicable for optical probes of radiating polarization sheets in such structures, for example, the photoluminescence from

two-dimensional (2D) transition metal dichalcogenides in a field-effect transistor[19].

We first consider radiation from the polarization sheet on top of a thin film, as illustrated in Fig. 1(a). A thin film of refractive index n_2 is sandwiched between two semi-infinite media, n_1 and n_3. Assuming an oscillating 2D polarization sheet of polarization $\mathbf{P}_s(\omega)$ at frequency ω is excited by beams incident from medium 1 and overlapping at boundary I [inset of Fig. 1(a)]. To find the electric field $\mathbf{E}(\omega)$ generated by $\mathbf{P}_s(\omega)$ in media 1 and 3, we employ boundary conditions of electromagnetic fields by using a 2D polarization sheet[18]. At boundary I

$$
\begin{aligned}
\Delta E_x = \sigma_z &= -\frac{4\pi}{\epsilon'}\mathrm{i}k_x P_{sz}, \\
\Delta E_y = \sigma_y &= 0, \\
\Delta H_x = \sigma_y &= -\frac{4\pi\mathrm{i}}{c}\omega P_{sy}, \\
\Delta H_y = \sigma_x &= \frac{4\pi\mathrm{i}}{c}\omega P_{sx},
\end{aligned}
\tag{1}
$$

where ϵ' is the effective dielectric constant of the interfacial layer[13], i is the square root of -1, $k = \omega/c$ is the light wave vector in a vacuum, and the lab coordinates (x, y, z) are set with z parallel to the surface normal $(\hat{n})$ and x–z is the beam incident plane [inset in Fig. 1(a)]. $\boldsymbol{\sigma}$ is the discontinuity in the electromagnetic field caused by $\mathbf{P}_s(\omega)$. For simplicity, we use the same symbol to represent different quantities in different cases. We define $\sigma_E \equiv 0$ and $\sigma_H \equiv \sigma_y$ for TE waves, and $\sigma_E \equiv \sigma_z$ and $\sigma_H \equiv \sigma_x$ for TM waves[18]. So, across boundary I, the relation between tangential components of the fields can be written as
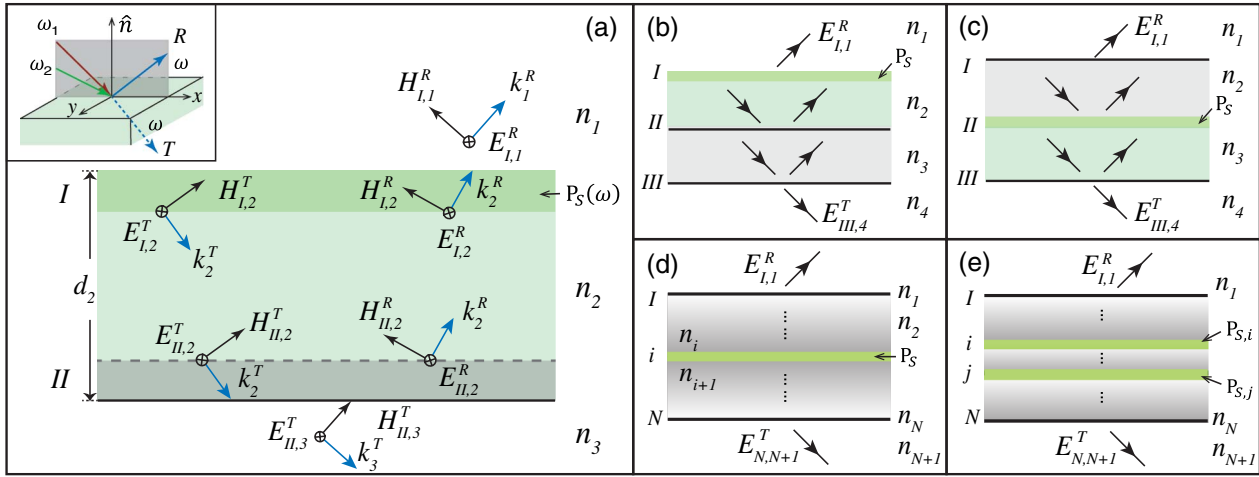
Fig. 1. (a) Electric (E) and magnetic (H) fields due to a radiating polarization sheet $\mathbf{P}_S(\omega)$ at the boundary I on top of a thin film of thickness d_2. k^R and k^T are beam wave vectors along the reflected and transmitted directions. Inset: Schematics of a typical experimental setup. (b), (c) Two-layer systems with $\mathbf{P}_S(\omega)$ at different boundaries. (d) An N-layer system with $\mathbf{P}_S(\omega)$ at the ith boundary between the ith and $(i+1)$th media. (e) An N-layer system with multiple interfacial polarization sheets.

$$E_{I,1} + \sigma_{I,E} = E_{I,2}, \quad H_{I,1} + \sigma_{I,H} = H_{I,2}, \qquad (2)$$

where $E_{I,i}$ ($H_{I,i}$) denotes the electric (magnetic) field inside the ith medium near boundary I. We denote the direction pointing from medium 1 to 3 as transmitted (T), and the other as reflected (R) [inset of Fig. 1(a)]. $\mathbf{E}(\omega)$ then has both T and R components in medium 2, but only the R component in medium 1, and the T component in medium 3. So inside medium 2, at boundary I,

$$E_{I,2} = E_{I,2}^R + E_{I,2}^T. \qquad (3a)$$

Since $\mathbf{H} = n\mathbf{k} \times \mathbf{E}$, we have

$$H_{I,2} = (E_{I,2}^T - E_{I,2}^R)\bar{n}_2, \qquad (3b)$$

where we define $\bar{n}_j = n_j \cos \beta_j$ for TE waves, and $\bar{n}_j = n_j / \cos \beta_j$ for TM waves, with n_i being the refractive index (complex in general) and β_i the beam refraction angle at ω in the ith medium. Combining Eqs. (2) and (3), we have

$$E_{I,1} + \sigma_{I,E} = E_{I,2}^R + E_{I,2}^T,$$
$$H_{I,1} + \sigma_{I,H} = (E_{I,2}^T - E_{I,2}^R)\bar{n}_2,$$

which can be written in the matrix form

$$\begin{bmatrix} E_{I,1} + \sigma_{I,E} \\ H_{I,1} + \sigma_{I,H} \end{bmatrix} = \begin{bmatrix} E_{I,2} \\ H_{I,2} \end{bmatrix} = \begin{bmatrix} 1 & 1 \\ \bar{n}_2 & -\bar{n}_2 \end{bmatrix} \begin{bmatrix} E_{I,2}^T \\ E_{I,2}^R \end{bmatrix}. \qquad (4a)$$

At boundary II, inside medium 2, the electric fields propagating along different directions are related to those at boundary I by $E_{I,2}^T = E_{II,2}^T \exp(-i\delta_2)$ and $E_{I,2}^R = E_{II,2}^R \exp(i\delta_2)$, where $\delta_2 = n_2 k \cos \beta_2 d_2$ is the propagation phase and d_2 is the thickness of medium 2.

The matrix form is

$$\begin{bmatrix} E_{I,2}^T \\ E_{I,2}^R \end{bmatrix} = \begin{bmatrix} \exp(-i\delta_2) & 0 \\ 0 & \exp(i\delta_2) \end{bmatrix} \begin{bmatrix} E_{II,2}^T \\ E_{II,2}^R \end{bmatrix}. \qquad (4b)$$

Toward medium 3, with no free charge, dipole, or current at the boundary, the tangential components of the fields across boundary II are related by

$$\begin{bmatrix} E_{II,3} \\ H_{II,3} \end{bmatrix} = \begin{bmatrix} E_{II,2} \\ H_{II,2} \end{bmatrix} = \begin{bmatrix} 1 & 1 \\ \bar{n}_2 & -\bar{n}_2 \end{bmatrix} \begin{bmatrix} E_{II,2}^T \\ E_{II,2}^R \end{bmatrix}. \qquad (4c)$$

Together, Eqs. (4a)–(4c) yield

$$\begin{bmatrix} E_{I,1} + \sigma_{I,E} \\ H_{I,1} + \sigma_{I,H} \end{bmatrix} = \begin{pmatrix} \cos \delta_2 & -\dfrac{i \sin \delta_2}{\bar{n}_2} \\ -i\bar{n}_2 \sin \delta_2 & \cos \delta_2 \end{pmatrix} \begin{bmatrix} E_{II,3} \\ H_{II,3} \end{bmatrix}$$
$$= \boldsymbol{M}_2 \begin{bmatrix} E_{II,3} \\ H_{II,3} \end{bmatrix}, \qquad (5a)$$

where $\boldsymbol{M}_2$ is the characteristic matrix of medium 2 as conventionally defined[19,20]. Moreover, since $E_{I,1} = E_{I,1}^R$, $H_{I,1} = -E_{I,1}^R \bar{n}_1$ and $E_{II,3} = E_{II,3}^T$, $H_{II,3} = -E_{II,3}^T \bar{n}_3$, Eq. (5a) can be rewritten as

$$\begin{bmatrix} E_{I,1}^R + \sigma_{I,E} \\ -E_{I,1}^R \bar{n}_1 + \sigma_{I,H} \end{bmatrix} = \boldsymbol{M}_2 \begin{bmatrix} E_{II,3}^T \\ -E_{II,3}^T \bar{n}_3 \end{bmatrix}. \qquad (5b)$$

This presents essentially two equations for two unknowns: $E_{I,1}^R$ and $E_{II,3}^T$, the reflected signal field in medium 1, and the transmitted field in medium 3, which are experimentally detectable with media 1 and 3 usually being the air or vacuum. Therefore, given the geometric and optical properties of all media, the signal fields can be solved from Eq. (5b) as functions of $\mathbf{P}_s(\omega)$.

As a quick check, we take $n_2 = n_3$ so that the system is equivalent to an oscillating polarization sheet between two semi-infinite media. For TE waves, for example, Eq. (5b) yields

$$E_{I,1,y}^R = \frac{4\pi i \omega}{c} \frac{1}{(\bar{n}_1 + \bar{n}_2)} \cdot P_{sy}^{(2)}, E_{II,3,y}^T$$

$$= \frac{4\pi i \omega}{c} \frac{1}{(\bar{n}_1 + \bar{n}_2)} \cdot P_{sy}^{(2)} e^{-i\delta_2},$$

which are identical with those in Refs. [13,18], and show the propagation phase in $E_{II,3,y}^T$ relative to $E_{I,1,y}^R$.

We now consider the case when the system is composed of more than one layer. For example, with an additional layer below medium 2 [Fig. 1(b)], the tangential fields at boundaries II and III are connected by

$$\begin{bmatrix} E_{II,2} \\ H_{II,2} \end{bmatrix} = \begin{bmatrix} E_{II,3} \\ H_{II,3} \end{bmatrix} = \boldsymbol{M}_3 \begin{bmatrix} E_{III,4} \\ H_{III,4} \end{bmatrix}, \tag{5c}$$

with $\boldsymbol{M}_3$ being the characteristic matrix of medium 3. Combining Eqs. (5a) and (5c), we then have

$$\begin{bmatrix} E_{I,1}^R + \sigma_{I,E} \\ H_{I,1}^R + \sigma_{I,H} \end{bmatrix} = \boldsymbol{M}_2 \boldsymbol{M}_3 \begin{bmatrix} E_{III,4}^T \\ H_{III,4}^T \end{bmatrix}. \tag{6a}$$

If the additional layer is above $\mathbf{P}_s(\omega)$, as the in geometry presented in Fig. 1(c), the tangential fields at boundaries I and III are then connected by

$$\begin{bmatrix} E_{I,1}^R \\ H_{I,1}^R \end{bmatrix} = \boldsymbol{M}_2 \begin{bmatrix} E_{II,2} \\ H_{II,2} \end{bmatrix},$$

$$\begin{bmatrix} E_{II,2} + \sigma_{II,E} \\ H_{II,2} + \sigma_{II,H} \end{bmatrix} = \begin{bmatrix} E_{II,3} \\ H_{II,3} \end{bmatrix} = \boldsymbol{M}_3 \begin{bmatrix} E_{III,4}^T \\ H_{III,4}^T \end{bmatrix}. \tag{6b}$$

Again, $E_{I,1}^R$ and $E_{III,4}^T$ can be readily solved from Eqs. (6a) and (6b). The above relations can be further generalized for any multilayer system. Assuming that the polarization sheet $\mathbf{P}_s(\omega)$ is at the ith boundary between the ith and $(i+1)$th media in a system of N layers, as illustrated in Fig. 1(d). Based on Eqs. (6a) and (6b), we have

$$\begin{bmatrix} E_{I,1}^R \\ -E_{I,1}^R \bar{n}_1 \end{bmatrix} = \left(\prod_{j=2}^{i} \boldsymbol{M}_j \right) \begin{bmatrix} E_{i,i} \\ H_{i,i} \end{bmatrix},$$

$$\begin{bmatrix} E_{i,i} + \sigma_{i,E} \\ H_{i,i} + \sigma_{i,H} \end{bmatrix} = \left(\prod_{j=i+1}^{N} \boldsymbol{M}_j \right) \begin{bmatrix} E_{N,N+1}^T \\ -E_{N,N+1}^T \bar{n}_{N+1} \end{bmatrix}. \tag{7}$$

Practically all $\boldsymbol{M}_i$ matrices can be computed given the composition of the multilayer structure. Then from Eq. (7), the signal fields $E_{I,1}^R$ and $E_{N,N+1}^T$ can be solved as functions of $\boldsymbol{\sigma}_i$, which is proportional to $\mathbf{P}_s(\omega)$.

Now we consider the case when there are more than one polarization sheets inside the multilayer structure. For example, assume there are two polarization sheets at the ith and jth boundaries [Fig. 1(e)], respectively. The total fields generated satisfy the equations

$$\begin{bmatrix} E_{I,1}^R \\ H_{I,1}^R \end{bmatrix} = \boldsymbol{M}_2 \cdots \boldsymbol{M}_i \begin{bmatrix} E_{i,i} \\ H_{i,i} \end{bmatrix},$$

$$\begin{bmatrix} E_{i,i} + \sigma_{i,E} \\ H_{i,i} + \sigma_{i,H} \end{bmatrix} = \boldsymbol{M}_{i+1} \cdots \boldsymbol{M}_j \begin{bmatrix} E_{j,j} \\ H_{j,j} \end{bmatrix},$$

$$\begin{bmatrix} E_{j,j} + \sigma_{j,E} \\ H_{j,j} + \sigma_{j,H} \end{bmatrix} = \boldsymbol{M}_{j+1} \cdots \boldsymbol{M}_N \begin{bmatrix} E_{N,N+1}^T \\ H_{N,N+1}^T \end{bmatrix}. \tag{8a}$$

Considering only the electric field generated by the ith polarization sheet, then we have

$$\begin{bmatrix} E'_{I,1} \\ H'_{I,1} \end{bmatrix} = \boldsymbol{M}_2 \cdots \boldsymbol{M}_i \begin{bmatrix} E'_{i,i} \\ H'_{i,i} \end{bmatrix},$$

$$\begin{bmatrix} E'_{i,i} + \sigma_{i,E} \\ H'_{i,i} + \sigma_{i,H} \end{bmatrix} = \boldsymbol{M}_{i+1} \cdots \boldsymbol{M}_j \begin{bmatrix} E'_{j,j} \\ H'_{j,j} \end{bmatrix},$$

$$\begin{bmatrix} E'_{j,j} \\ H'_{j,j} \end{bmatrix} = \boldsymbol{M}_{j+1} \cdots \boldsymbol{M}_N \begin{bmatrix} E'_{N,N+1} \\ H'_{N,N+1} \end{bmatrix}. \tag{8b}$$

Similarly, the electric field generated by the jth polarization sheet is

$$\begin{bmatrix} E''_{I,1} \\ H''_{I,1} \end{bmatrix} = \boldsymbol{M}_2 \cdots \boldsymbol{M}_i \begin{bmatrix} E''_{i,i} \\ H''_{i,i} \end{bmatrix},$$

$$\begin{bmatrix} E''_{i,i} \\ H''_{i,i} \end{bmatrix} = \boldsymbol{M}_{i+1} \cdots \boldsymbol{M}_j \begin{bmatrix} E''_{j,j} \\ H''_{j,j} \end{bmatrix},$$

$$\begin{bmatrix} E''_{j,j} + \sigma_{j,E} \\ H''_{j,j} + \sigma_{j,H} \end{bmatrix} = \boldsymbol{M}_{j+1} \cdots \boldsymbol{M}_N \begin{bmatrix} E''_{N,N+1} \\ H''_{N,N+1} \end{bmatrix}, \tag{8c}$$

respectively. By summing up the corresponding equations in Eqs. (8b) and (8c), we have

$$\begin{bmatrix} E'_{I,1} + E''_{I,1} \\ H'_{I,1} + H''_{I,1} \end{bmatrix} = \boldsymbol{M}_2 \cdots \boldsymbol{M}_i \begin{bmatrix} E'_{i,i} + E''_{i,i} \\ H'_{i,i} + H''_{i,i} \end{bmatrix},$$

$$\begin{bmatrix} E'_{i,i} + E''_{i,i} + \sigma_{i,E} \\ H'_{i,i} + H''_{i,i} + \sigma_{i,E} \end{bmatrix} = \boldsymbol{M}_{i+1} \cdots \boldsymbol{M}_j \begin{bmatrix} E'_{j,j} + E''_{j,j} \\ H'_{j,j} + H''_{j,j} \end{bmatrix},$$

$$\begin{bmatrix} E'_{j,j} + E''_{j,j} + \sigma_{j,E} \\ H'_{j,j} + H''_{j,j} + \sigma_{j,E} \end{bmatrix} = \boldsymbol{M}_{j+1} \cdots \boldsymbol{M}_N \begin{bmatrix} E'_{N,N+1} + E''_{N,N+1} \\ H'_{N,N+1} + H''_{N,N+1} \end{bmatrix}. \tag{8d}$$

Clearly, Eq. (8d) is equivalent to Eq. (8a), with $E_{I,1}^R = E'_{I,1} + E''_{I,1}$. Therefore, we verify that the overall

signal is the superposition of those from the individual sheets. One can either solve the total fields directly from Eq. (8a), or first calculate them from each polarization sheet, and then get the total fields by summing them up [Eqs. (8b)–(8d)]. As the contribution from each individual sheet is obtained analytically, we can then design the multilayer structure to selectively boost up and/or suppress responses from specific positions. When there are steps and terraces on the surface, if the scattering is not significant, it can be modeled as an ensemble of films with various thickness; and given the thickness distribution, we can still apply the same method to estimate the local electric fields. In the following, we present two practical examples as a demonstration.

Thin films of nonlinear optical materials are commonly used for reference signal generation, upconversion detection, etc.[21–23]. Compared to bulk nonlinear crystals, thin films can support a much greater bandwidth, but may suffer from low efficiency due to the limited beam interaction length. Nonetheless, we can also increase the local electric field with appropriate film thicknesses with the interference. In the following example, we calculate the second harmonic (SH) fields generated by a nonlinear thin film of thickness d deposited on a dielectric substrate. We assume that the fundamental beam ω is incident from the air side at $45°$ and generates SH beams at 2ω [Fig. 2(a)]. At position z' inside the film, the nonlinear polarization at 2ω in a slab of thickness d is[24]

$$\mathrm{d}\boldsymbol{P}_S^{(2)}(2\omega, z') = \boldsymbol{P}_B^{(2)}(2\omega, z')\mathrm{d}z'$$
$$= \overset{\leftrightarrow}{\chi}_B^{(2)}(2\omega, z'){:}\boldsymbol{E}(\omega, z')\boldsymbol{E}(\omega, z')\mathrm{d}z', \qquad (9)$$

where $\overset{\leftrightarrow}{\chi}_B^{(2)}$ is the bulk second-order nonlinear susceptibility of the material. The total response is the integration of that from all $\mathrm{d}\boldsymbol{P}_S^{(2)}(2\omega, z')$ along the z direction. The local strength of the input field $\boldsymbol{E}(\omega, z')$ can be calculated from the standard characteristic matrix formalism[16,19,20]. The
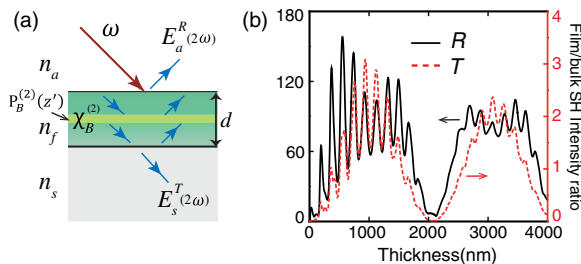

(a) Schematics of SHG from a nonlinear thin film on a substrate. (b) The calculated ratio between the SH signal from the thin film and that from a bulk nonlinear crystal versus the film thickness, detected along the reflected (solid line) or transmitted directions (dashed curve). The incident beam is centered at 800 nm with a bandwidth of 60 nm. All beams are TE waves.
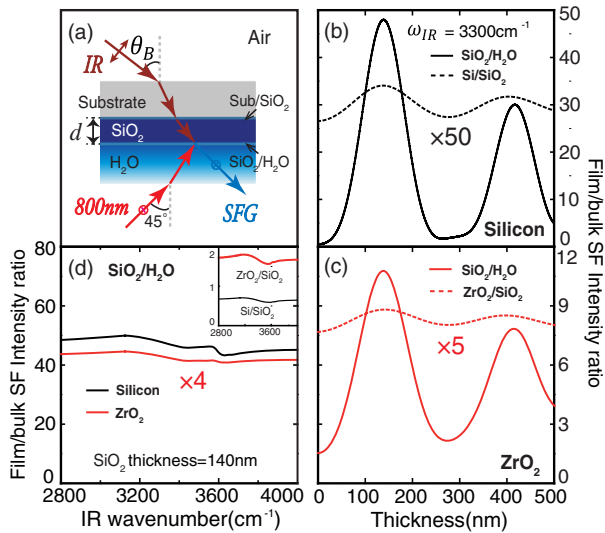
signal fields generated by $\mathrm{d}\boldsymbol{P}_S^{(2)}(2\omega, z')$ outside the film can be obtained using Eq. (9), that is

$$\begin{bmatrix} \mathrm{d}E_a^R(z') \\ -\mathrm{d}E_a^R(z')\bar{n}_a \end{bmatrix} = \boldsymbol{M}_f(z')\begin{bmatrix} \mathrm{d}E_f(z') \\ \mathrm{d}H_f(z') \end{bmatrix},$$
$$\begin{bmatrix} \mathrm{d}E_f(z') + \mathrm{d}\boldsymbol{\sigma}_E(z') \\ \mathrm{d}H_f(z') + \mathrm{d}\boldsymbol{\sigma}_H(z') \end{bmatrix} = \boldsymbol{M}_f(d - z')\begin{bmatrix} \mathrm{d}E_s^T(z') \\ -\mathrm{d}E_s^T(z')\bar{n}_s \end{bmatrix}, \quad (10)$$

where $\mathrm{d}\boldsymbol{\sigma}(z')$ are related to $\mathrm{d}\boldsymbol{P}_S^{(2)}(2\omega, z')$ as in Eq. (1), and subscripts a, f, and s stand for air, film, and substrate, respectively. $\boldsymbol{M}_f(z')$ is the characteristic matrix of the layer between the air/film interface and the polarization sheet at z', and $\boldsymbol{M}_f(d - z')$ equals that of the layer between z' and the substrate [Fig. 2(a)]. We can then obtain $\mathrm{d}E_a^R(z')$ and $\mathrm{d}E_s^T(z')$ by solving Eq. (10). For simplicity, we consider only the TE mode[15,16,24], and we find

$$\mathrm{d}E_{a,y}^R(z') = \frac{\bar{n}_f \cos \delta_{d-z'} - \mathrm{i}\bar{n}_s \sin \delta_{d-z'}}{\epsilon_+ \cos \delta_d - \mathrm{i}\epsilon_- \sin \delta_d} \cdot \mathrm{d}\sigma_{H,y}(z'),$$
$$\mathrm{d}E_{s,y}^T(z') = \frac{\bar{n}_f \cos \delta_{z'} - \mathrm{i}\bar{n}_a \sin \delta_{z'}}{\epsilon_+ \cos \delta_d - \mathrm{i}\epsilon_- \sin \delta_d} \cdot \mathrm{d}\sigma_{H,y}(z'),$$

where $\epsilon_+ = \bar{n}_a\bar{n}_f + \bar{n}_f\bar{n}_s$, $\epsilon_- = \bar{n}_a\bar{n}_s + \bar{n}_f^2$, and $\delta_{z'} = n_f k \cos \beta_f z'$ is the beam propagation phase through a medium of thickness z'. The total SH field from the film is:

$$E_{a,y}^R = \int_0^d \mathrm{d}E_{a,y}^R(z'), \ E_{s,y}^T = \int_0^d \mathrm{d}E_{s,y}^T(z').$$

Numerically, we consider an LiNbO$_3$ film (anisotropy neglected) on an SiO$_2$ substrate with an excitation centered at 800 nm (ω_c), and a bandwidth of 60 nm, which corresponds to about a 35 fs pulse duration. Figure 2(b) presents the ratio between SH intensities from the thin film ($d \leq 4000$ nm) and from a bulk crystal ($d \to \infty$) along both the reflected and transmitted directions. Strong enhancement can be achieved for $d \sim 1000$ and ~ 3000 nm. Specifically, the signal can be enhanced by more than 100 times along the reflected direction. The curves are characterized by oscillations due to the interference between multiply reflected beams. The small period of 190 nm $\sim 2\pi c/(2\omega_c n_f \cos \theta_f)$ is due to the SH beam, and the large period of 2070 nm $\sim 2\pi/\Delta k = 2\pi/|k_{fz}(2\omega) - 2k_{fz}(\omega)|$ is due to the wave vector mismatch between the fundamental and SH beams[14]. It is also seen that the small period oscillation diminishes in thicker films [Fig. 2(b)]. This is because of the beating between different frequency components, which run out of phase when d increases. The second example is regarding the sum-frequency (SF) spectroscopy on interfaces. In many cases, the moiety of interest yields very weak signals, such as reaction intermediates[25] or excited species in ultrafast dynamic studies[26]. So it is desirable to enhance SF signals without changing the surface structure of interest. Here, we consider the widely studied interface between water and SiO$_2$, which has served as a model system of mineral/water interfaces, but often suffers from weak SF signals[27]. The proposed structure

Fig. 3. (Color online) (a) Schematic of SFG from substrate/ SiO_2/water system. (b), (c) The calculated ratio between the SF signals from the thin film SiO_2/H_2O interface to that from a bulk SiO_2/H_2O interface, versus the SiO_2 film thickness (solid lines). The signal ratio from the substrate/SiO_2 interface is shown for comparison (dashed lines, magnified for clarity). The substrate material is assumed to be (b) silicon or (c) cubic zirconia. The infrared wavenumber is at 3300 cm^{-1}. (d) The spectral dependence of SF signals from a 140 nm thick SiO_2/H_2O interface, deposited on silicon (black) or cubic zirconia (red). The inset shows that from the substrate/SiO_2 interfaces.

is to sandwich a thin SiO_2 layer of thickness d between water and a dielectric substrate [Fig. 3(a)]. We assume a P-polarized broadband mid-infrared (IR) beam incident at the Brewster angle, and an S-polarized near-IR beam at 800 nm from the water side at 45°, and we probe S-polarized SF output from the water side. Figures 3(b) and 3(c) display the ratio between SF intensities from the water interface with a thin film SiO_2 ($d \leq 500$ nm), and with a bulk SiO_2 ($d \to \infty$). Two different substrate materials, silicon [Si, Fig. 3(b)] and cubic zirconia [ZrO_2, Fig. 3(c)], were used and the mid-IR frequency 3300 cm^{-1} was central to the OH-stretch vibration regime[26]. It is seen that at $d\sim$140 nm, the SF signal can be enhanced by about 50 times with the Si substrate, and more than 10 times with ZrO_2. To confirm that the substrate/SiO_2 interface does not cause complications, we also evaluated its relative contributions (dashed lines), which turned out to be negligible compared the interface of interest. Finally, we calculated the spectral dependence of the local field intensity at $d = 140$ nm [Fig. 3(d)], which remains nearly a constant in the entire OH-stretch vibration regime, so will not cause spectral distortion. Therefore, with the appropriate choice of substrate material and SiO_2 layer thickness, we can effectively enhance SF signals from the SiO_2/water interface.

In conclusion, we present a general and analytical method to calculate the local electric field across a multilayer structure of arbitrary composition that can facilitate the quantitative analysis as well as geometric optimization

for optical studies on such systems. With two practical examples, we show that an optimized multilayer structure can effectively enhance the nonlinear response of interest.

References

1. M.-H. Chiu, C. Zhang, H.-W. Shiu, C.-P. Chuu, C.-H. Chen, C.-Y. S. Chang, C.-H. Chen, M.-Y. Chou, C.-K. Shih, and L.-J. Li, Nat. Commun. **6**, 7666 (2015).
2. S. Héron, P. Bouchon, and R. Haïdar, Phys. Rev. A **94**, 033831 (2016).
3. J. Zhao, H. He, H. Wang, K. Yi, B. Wang, and Y. Cui, Chin. Opt. Lett. **14**, 083401 (2016).
4. J. Liu, W. Zhang, H. Cui, J. Sun, H. Li, K. Yi, and M. Zhu, Chin. Opt. Lett. **12**, 083101 (2014).
5. M. Sieger and B. Mizaikoff, Photon. Res. **4**, 106 (2016).
6. E. Feigenbaum, K. Diest, and H. A. Atwater, Nano Lett. **10**, 2111 (2010).
7. M.-X. Wang, C. Liu, J.-P. Xu, F. Yang, L. Miao, M.-Y. Yao, C. L. Gao, C. Shen, X. Ma, X. Chen, Z.-A. Xu, Y. Liu, S.-C. Zhang, D. Qian, J.-F. Jia, and Q.-K. Xue, Science **336**, 52 (2012).
8. W. T. Liu and Y. R. Shen, Proc. Natl. Acad. Sci. U. S. A. **111**, 1293 (2014).
9. T. Jiang, H. Liu, D. Huang, S. Zhang, Y. Li, X. Gong, Y.-R. Shen, W.-T. Liu, and S. Wu, Nat. Nanotechnol. **9**, 825 (2014).
10. H.-F. Wang, Prog. Surf. Sci. **91**, 155 (2016).
11. D. A. Kopylov, S. E. Svyakhovskiy, L. V. Dergacheva, V. A. Bushuev, B. I. Mantsyzov, and T. V. Murzina, Phys. Rev. A **93**, 053840 (2016).
12. Y. Cao, S. Chen, Y. Li, Y. Gao, D. Yang, Y. R. Shen, and W. T. Liu, Sci. Adv. **2**, e1601162 (2016).
13. X. Zhuang, D. Kim, P. Miranda, and Y. R. Shen, Phys. Rev. B Condens. Matter **59**, 12632 (1999).
14. W.-T. Liu and Y. R. Shen, Phys. Rev. B **78**, 024302 (2008).
15. X. Lu, M. L. Clarke, D. Li, X. Wang, G. Xue, and Z. Chen, J. Phys. Chem. C **115**, 13759 (2011).
16. H. Shi, Y. Zhang, M. Yao, F. Ji, D. Qian, S. Qiao, Y. R. Shen, and W.-T. Liu, Phys. Rev. B **94**, 205307 (2016).
17. M. C. Larciprete, A. Belardini, M. G. Cappeddu, D. de Ceglia, M. Centini, E. Fazio, C. Sibilia, M. J. Bloemer, and M. Scalora, Phys. Rev. A **77**, 013809 (2008).
18. Y. R. Shen, *The Principles of Nonlinear Optics* (Wiley-Interscience, 2003).
19. O. Arnon and P. Baumeister, Appl. Opt. **19**, 1853 (1980).
20. M. Born and E. Wolf, *Principles of Optics* (Cambridge University Press, 1999).
21. V. N. Konopsky, E. V. Alieva, S. Y. Alyatkin, A. A. Melnikov, S. V. Chekalin, and V. M. Agranovich, Light Sci. Appl. **5**, e16168 (2016).
22. I. P. Kaminow, J. R. Carruthers, E. H. Turner, and L. W. Stulz, Appl. Phys. Lett. **22**, 540 (1973).
23. Z. C. Tiu, H. Ahmad, A. Zarei, and S. W. Harun, Chin. Opt. Lett. **14**, 041901 (2016).
24. D. Wilk, D. Johannsmann, C. Stanners, and Y. R. Shen, Phys. Rev. B **51**, 10057 (1995).
25. D. Lis, E. H. Backus, J. Hunger, S. H. Parekh, and M. Bonn, Science **344**, 1138 (2014).
26. J. A. McGuire and Y. R. Shen, Science **313**, 1945 (2006).
27. A. Myalitsin, S.-H. Urashima, S. Nihonyanagi, S. Yamaguchi, and T. Tahara, J. Phys. Chem. C **120**, 9357 (2016).